TISSUE ENGINEERING: Part C
Volume 25, Number 5, 2019

DOI: 10.1089/ten.tec.2018.0339

termis
Tissue Engineering
& Regenerative Medicine
International Society

METHODS ARTICLE

Fabrication and Characterization of Electrospun Decellularized Muscle-Derived Scaffolds

Mollie M. Smoak, BS,[1] Albert Han,[1] Emma Watson, BS,[1] Alysha Kishan, PhD,[2] K. Jane Grande-Allen, PhD,[1] Elizabeth Cosgriff-Hernandez, PhD,[2] and Antonios G. Mikos, PhD[1]

Although skeletal muscle has a high potential for self-repair, volumetric muscle loss can result in impairment beyond the endogenous regenerative capacity. There is a clinical need to improve on current clinical treatments that fail to fully restore the structure and function of lost muscle. Decellularized extracellular matrix (dECM) scaffolds have been an attractive platform for regenerating skeletal muscle, as dECM contains many biochemical cues that aid in cell adhesion, proliferation, and differentiation. However, there is limited capacity to tune physicochemical properties in current dECM technologies to improve outcome. In this study, we aim to create a novel, high-throughput technique to fabricate dECM scaffolds with tunable physicochemical properties while retaining proregenerative matrix components. We demonstrate a successful decellularization protocol that effectively removes DNA. We also identified key steps for the successful production of electrospun muscle dECM without the use of a carrier polymer; electrospinning allows for rapid scaffold fabrication with high control over material properties, which can be optimized to mimic native muscle. To this end, fiber orientation and degree of crosslinking of these dECM scaffolds were modulated and the corollary effects on fiber swelling, mechanical properties, and degradation kinetics were investigated. Beyond application in skeletal muscle, the versatility of this technology has the potential to serve as a foundation for dECM scaffold fabrication in a variety of tissue engineering applications.

Keywords: extracellular matrix, decellularized muscle, electrospinning, skeletal muscle

Impact Statement

This study develops a method to decellularize skeletal muscle and fabricate electrospun scaffolds from the decellularized tissue without the need for a carrier polymer. In addition, the resulting scaffolds have tunable physicochemical properties, including fiber alignment, while retaining important extracellular matrix components for regeneration of skeletal muscle.

Introduction

Skeletal muscle constitutes ~40% of total body weight and makes up the largest tissue mass in the body.[1] Although skeletal muscle has a high potential for self-repair in acute injuries, volumetric muscle loss (VML) due to trauma or surgical intervention results in impairment of function beyond the endogenous regenerative capacity.[2,3] Such injuries prove difficult to treat clinically, often leading to complications and permanent loss of limb function. The current surgical standard for treatment involves transfer of an autologous muscle flap paired with physical therapy.[4] However, use of autografts can lead to donor-site morbidity and increased recovery time. This, as well as other current treatment options, falls short of restoring structure and function of lost muscle.[5] In compound injuries, such as those involving muscle and bone, the impairment of muscle can also lead to reduced healing of neighboring tissues.[6,7] VML affects a high number of civilian and military men and women each year.[3–5] Therefore, there is a great need for the development of an improved therapeutic option to regenerate muscle following VML.

Tissue-engineered scaffolds hold significant potential in addressing this issue. Scaffolds have been commonly used to promote and guide regeneration of impaired tissue by providing an artificial extracellular matrix (ECM) for cells. These scaffolds are designed to be biocompatible and mimic properties of the tissue they replace to allow for cell adhesion, proliferation, differentiation, and retention of important proteins and growth factors.[1–9] A wide range of biomaterials and fabrication processes have been developed to accommodate

[1]Department of Bioengineering, Rice University, Houston, Texas.
[2]Department of Biomedical Engineering, University of Texas, Austin, Texas.

the various physicochemical and biological properties that are desirable to support cells.

In the last several years, the use of decellularized tissues has gained interest and become an attractive platform for the regeneration of skeletal muscle.[10–14] Therapies that utilize decellularized extracellular matrix (dECM) involve harvesting tissue from a donor or host, exposing the tissue to detergents to remove nuclear acids and other unwanted donor material that may elicit an unwanted immune response, and processing the tissue into a usable form for transplantation.[15] Such methods have shown promise in VML models because dECM retains the necessary biochemical cues to promote cell recruitment, proliferation, and differentiation.[2,16,17] In addition to eliciting a myogenic response, muscle dECM has been shown to promote vascular formation and reinnervation in VML models,[17] processes that are critical for function and historically difficult to induce in VML treatments. However, there remain obstacles in modulating the physicochemical properties of dECM and scaling such materials to clinically relevant shapes and sizes.

Many scientists have sought to overcome these obstacles by enzymatically digesting these materials and taking advantage of their natural thermoresponsive properties to generate hydrogel scaffolds.[10–12,18] dECM hydrogels have made great strides in controlling the size and shape of dECM scaffolds. In addition, hydrogels can be crosslinked or further modified to have some control over material properties. However, the digestion required for hydrogel formation often inactivates important ECM components.[19] There is also limited control over the internal architecture of the material. Myogenic differentiation and the formation of mature myotubes have proven to be very challenging because of the need for moderate tensile mechanical properties and highly aligned internal architecture. For this reason, electrospinning may provide a better alternative for fabrication of dECM scaffolds that allow for modulation of architecture and mechanical properties for myogenic differentiation.

Electrospinning allows for high-throughput production of nano- and microscale fibers with high control over fiber diameter and alignment as well as bulk scaffold porosity.[20–23] Postprocessing steps have also been developed to modulate the degree of crosslinking of electrospun natural polymers to provide additional control of mechanical properties and resorption rate.[24–26] In addition, the inherent porosity of electrospun scaffolds mimics native ECM and facilitates exchange of nutrients and metabolic waste. Recent studies have reported dECM blended with synthetic polymers to create hybrid scaffolds with enhanced biochemical properties compared with traditional synthetic materials.[27–32] However, dECM alone has been shown to be difficult to electrospin and produce stable scaffolds for analysis. To our knowledge, there are no current studies in the literature of successful electrospinning of muscle dECM without a carrier polymer. While synthetic polymers are often crucial to control degradation and mechanical properties, a material completely derived from natural materials may be ideal for mimicking the native cell microenvironment.[33]

In this work, we developed a novel method for fabricating electrospun muscle dECM scaffolds that are effectively decellularized and retain key ECM components. We investigated the effects of fiber orientation and the degree of crosslinking on fiber swelling as well as bulk scaffold swelling, porosity, tensile properties, and degradation kinetics. Scaffolds were imaged via confocal microscopy in both the dry state and after swelling in saline solution to evaluate fiber swelling and porosity. Tensile mechanical properties were assessed via a uniaxial mechanical testing machine in an aqueous testing chamber, and degradation kinetics was evaluated in saline and collagenase solutions.

Materials and Methods

Decellularization of skeletal muscle tissue

Male New Zealand White rabbits were donated from the University of Texas Health Science Center at Houston in accordance with protocols approved by the University of Texas Health Science Center at Houston Institutional Animal Care and Use Committee. Muscle tissue was harvested from the hind legs of male New Zealand White rabbits. The fascia and visible connective tissue were removed, and the tissue was washed in sterile ultrapure water supplemented with 1% penicillin/streptomycin (Sigma-Aldrich, St. Louis, MO) overnight at 4°C. Centrifugation at 5000 rpm for 3 min was used for all media changes. All media changes were performed under sterile conditions. Tissue samples were trimmed to ~3 mm in thickness and subsequently immersed in an enzyme solution of phosphate-buffered saline (PBS), 0.025% trypsin (Sigma-Aldrich), and 0.05% ethylenediaminetetraacetic acid (EDTA) (Sigma-Aldrich) and agitated for 1 h at room temperature. The tissue was then washed two times in PBS. Muscle samples were then placed in 1% Triton X-100 (Sigma-Aldrich) supplemented with 1% antibiotic and agitated overnight at 4°C. The muscle was then washed twice with PBS, followed by treatment with hypotonic (10 mM tris-HCl) and hypertonic (50 mM tris-HCl and 1.5 M NaCl) salt solutions. Muscle samples were agitated in hypertonic/hypotonic solutions supplemented with 1% penicillin/streptomycin in 30-min increments at room temperature. These solutions were cycled through a minimum of three times, and samples were further cut if tissue core remained colored after two cycles. Once the tissue turned completely white, it was washed in ultrapure water for an additional 24 h to remove any salt solution. The decellularized muscle (dECM) was then homogenized using a variable speed tissue homogenizer, and the slurry was frozen and dried.

Experimental design

To investigate the versatility of the dECM electrospinning system as it applies for muscle tissue engineering, we chose to modulate fiber orientation and crosslinking density of electrospun dECM scaffolds. We used a full factorial design and characterized four groups of electrospun dECM scaffolds—randomly oriented, uncrosslinked (RO); randomly oriented, crosslinked (ROX); aligned, uncrosslinked (AO); and aligned, crosslinked (AOX). The extremes of fiber alignment and crosslinking density were chosen to observe the extreme effects on physicochemical properties.

Electrospinning dECM fibers

After decellularization and complete drying, the homogenized muscle samples were ground into a fine powder and sieved to remove any particles larger than 300 μm.

Electrospinning solutions were then prepared by adding dECM powder to chilled hexafluro-2-propanol (HFIP) (Sigma-Aldrich) with constant stirring to ensure even dispersion of particles without aggregation. The dECM/HFIP (10%, w/v) solution was then stirred overnight at 4°C. To form random fibers, dECM/HFIP was electrospun onto a stationary plate at a flow rate of 1 mL/h using a 22G blunted needle. The collector carried a negative voltage of −2 kV and was placed ~15 cm away from the electrospinning needle, which carried a positive voltage of 7 kV. Electrospinning continued until the mesh reached the desired thickness.

Aligned fibers were formed by electrospinning dECM/HFIP onto a rotating drum at ~10.5 m/s (Yflow® professional electrospinning machine, Málaga, Spain). The electrospinning solution was extruded from a blunted 18G needle at a flow rate of 2.5 mL/h. The inverted needle carried a voltage of ~17 kV and was placed ~10 cm from the rotating drum, which carried a voltage of approximately −3 kV. Electrospinning continued until the mesh reached a desired thickness. On completion, all meshes were dried, purged with nitrogen, and stored at 4°C until use. Biopsy punches were then used to create circular scaffolds of varying diameters.

For groups that required crosslinking (ROX and AOX), scaffolds were carefully placed inside a desiccator, ensuring that scaffolds did not overlap one another. Glutaraldehyde (25%) was then poured into a glass dish and placed inside the desiccator beside the electrospun scaffolds. The desiccator was then sealed and placed under vacuum for 24 h. After crosslinking, the scaffolds were allowed to vent overnight to remove any residual glutaraldehyde.[24]

Biochemical characterization of dECM

Quantification of DNA. To determine the extent of decellularization, residual DNA content was measured. Dried dECM powder, RO electrospun dECM scaffolds, and dried, untreated rabbit tissue were first lysed in proteinase K solution (100 μg/mL) for 24 h at 60°C with intermittent agitation. DNA was then isolated by first centrifuging lysed samples at 10,000 *g* for 10 min at 4°C.[10] The supernatant was then removed from precipitated material and incubated with phenol/chloroform (V:V = 1:1) for 10 min under agitation. The solution was then centrifuged at 10,000 *g* for 30 min at 4°C. The aqueous phase was then removed and added to 3 M sodium acetate and ethanol. The DNA was allowed to precipitate overnight at 4°C. The solution was then centrifuged at 10,000 *g* for 10 min at 4°C. The precipitate was dried and resuspended in ultrapure water. DNA content was determined via a PicoGreen assay kit (Invitrogen, Carlsbad, CA). The PicoGreen kit was used in accordance with the manufacturer's guidelines. The fluorescence intensity was read using a fluorescence plate reader (BioTek, Winooski, VT; excitation wavelength: 485 nm; emission wavelength: 528 nm). The DNA standard curve was generated using lambda DNA standards obtained from the PicoGreen kit.

Quantification of total protein. Dried dECM powder, RO electrospun dECM scaffolds, and dried, untreated rabbit tissue were suspended in ultrapure water and solubilized using a tissue lyser (Qiagen, Hilden, Germany). Total protein of the samples was then measured via a bicinchoninic acid (BCA) assay kit (Thermo Scientific™, Waltham, MA). The BCA kit was used in accordance with the manufacturer's guidelines. The tissue samples and albumin controls were incubated for 2 h at 37°C. The plate was then cooled, and absorbance was read at 562 nm on a plate reader (BioTek).

Quantification of sulfated glycosaminoglycans. Dried dECM powder, RO electrospun dECM scaffolds, and dried, untreated rabbit tissue were first lysed in proteinase K solution (100 μg/mL) for 24 h at 60°C with intermittent agitation. Sulfated glycosaminoglycan (sGAG) content was then measured via a 1,9-dimethylmethylene blue (DMMB) assay. Each sample/standard was added to a microcentrifuge tube. Working solution was made fresh using 5 mL of formate solution (2.5 g sodium formate, 240 mL of 1 M guanidine hydrochloride, and 2.795 mL of 85% formic acid), 1.25 mL of DMMB solution (0.64 mg DMMB/mL ethanol), and 18.75 mL of ultrapure water. After the addition of working solution, the tubes were mixed at low levels for 30 min and centrifuged at 12,000 rpm for 10 min to form and precipitate the sGAG-dye complex. After carefully draining the tubes, decomplexation solution (2.05 g sodium acetate, 50 mL isopropanol, 250 mL of 8 M guanidine hydrochloride, and 200 mL ultrapure water) was added to each tube. Tubes were vortexed until all bound dye was dissolved. Solutions were then transferred to a microplate, and absorbance was read at 656 nm on a plate reader (BioTek). A standard curve was generated using chondroitan-4 sulfate at 0–5 μg/100 μL.

Quantification of collagen. Dried dECM powder, RO electrospun dECM scaffolds, and dried, untreated rabbit tissue were suspended in ultrapure water and solubilized using a tissue lyser. Collagen content was measured via a previously established hydroxyproline assay.[34] Samples were placed in autoclave-safe tubes and hydrolyzed by adding 10 N NaOH and autoclaving for 20 min at 121°C. Samples were then cooled and neutralized using 10 N HCl. The plate was then incubated at room temperature in chloramine-T solution for 20 min to allow for oxidation. P-dimethyl-amino-benzaldehyde solution was then added and the plate was incubated for 30 min at 60°C to develop. The plate was then cooled, and absorbance was read at 570 nm on a plate reader (BioTek). The resulting hydroxyproline concentration for each sample was then converted to collagen concentration following a 1:10 ratio of hydroxyproline to collagen.[35]

Identification of proteins within dECM scaffolds. Electrospun scaffolds from three different rabbits were sent to Baylor College of Medicine Proteomics Core Facility (Houston, TX), and liquid chromatography with tandem mass spectrometry (LC-MS/MS) was run. The area coverage for each protein was then averaged ($n = 3$) and reported as a percentage of the average total protein area coverage.

Histological evaluation of decellularized muscle

Decellularized muscle tissue was submerged in Histoprep frozen tissue embedding media (Sigma-Aldrich), and samples were frozen overnight. Cryosectioning was used to cut

embedded tissues into 20 μm sections. The sections were then fixed with 10% formalin and exposed to Bouin's solution for 1 h at 60°C. After rinsing, sections were stained for collagen using an Alcian blue stain and imaged.

Evaluation of fiber swelling via confocal microscopy

Four groups of dECM scaffolds were tested for fiber swelling (RO, ROX, AO, and AOX). Confocal microscopy was used to evaluate fiber swelling. To measure dry fiber diameter, fluorescein was added to dECM electrospinning solutions and electrospun to incorporate the fluorophore within single fibers. Scaffolds were then dried and imaged dry using a confocal microscope (Zeiss 5 Live). Areas imaged were randomly selected within five zones on the scaffold (center, upper right, upper left, lower right, and lower left) before examining the fibers in those areas to minimize bias. In ImageJ, a line was then drawn through the center of each image, and the fiber diameter of all fibers ($n \geq 10$) intersecting this line was measured. This analysis was repeated for each of the five zones, and the fiber diameter was reported as an average of all fibers measured in the five images ($n \geq 50$). To measure swollen fiber diameter, scaffolds were submerged in PBS for 24 h. Scaffolds were incubated in fluorescein during the last 30 min of their swelling time. The scaffolds were then imaged and evaluated in the same manner as the dry scaffolds.

Evaluation of bulk scaffold swelling

The bulk scaffold swelling of all four groups of dECM scaffolds was evaluated. The dECM was cut into scaffolds of ~10 mm in diameter. The thickness of each scaffold was tested using a mechanical testing machine in a compression configuration. Dry scaffolds were placed atop a glass slide on the bottom clamp attached to the load cell of the mechanical tester. The top clamp was then moved downward toward the bottom clamp. When the clamp contacted the scaffold and the load cell achieved a force of 0.025 g downward, the movement was stopped and the distance of the top clamp was recorded. This analysis was repeated for all scaffolds within each group. All distances were subtracted from the distance that the top clamp moved to the glass slide without the presence of any material. Scaffolds were then swollen in PBS for 24 h, and their thickness was measured again.

The scaffold diameter was also measured dry and after swelling in PBS. Dry scaffolds were placed between two microscope slides and positioned beside a standard ruler. The scaffolds were then imaged with a stereomicroscope. This process was repeated with swollen scaffolds. Images were then analyzed in ImageJ image processing software. The boundaries of the scaffolds were defined, and the Feret diameter was measured for each image.

Porosity of dECM scaffolds

The porosity of dECM scaffolds was evaluated for the four groups (RO, ROX, AO, and AOX). Confocal z-stacks (0.48 μm step intervals) were taken in each group using the zone method described for fiber swelling measurements. The z-stacks were then analyzed via ImageJ image processing software. Thresholding was performed for each stack of images to isolate the dECM fibers (representative images shown in Supplementary Fig. S1). The area of the fibers (white pixels), A_{fiber}, was then measured and divided by the total area (white + black pixels), A_{total}. This analysis was performed for each image slice in the stack and averaged for each z-stack. A minimum of five slices were used for each z-stack. The porosity was then calculated by the following equation:

$$\varepsilon = 1 - \frac{A_{fiber}}{A_{total}}$$

Degradation kinetics of dECM scaffolds

The degradation kinetics of the four groups was tested (RO, ROX, AO, and AOX) in two different media. PBS was used to model degradation of dECM scaffolds via hydrolysis. PBS supplemented with collagenase (125 U/mL) was used to model enzymatic degradation.[36] Circular scaffolds (10 mm Ø) were dried and weighed before exposure to degradation medium. Scaffolds were then placed in 3 mL of degradation medium and incubated at 37°C under mild agitation. Degradation media were changed twice per week over the course of the study. At the completion of a time point, the media were removed from the respective scaffolds, and the scaffolds were frozen, dried, and weighed. The final weight was reported as a percentage of the initial weight before the start of the study.

Mechanical testing of dECM scaffolds

A uniaxial tensile mechanical testing machine equipped with a room temperature aqueous testing chamber was used to measure the tensile modulus of each dECM group (RO, ROX, AO, and AOX) as well as untreated rabbit skeletal muscle. The electrospun dECM was cut into 10×50 mm strips (0.2 ± 0.1 mm thickness). Aligned scaffolds were marked parallel to the fiber orientation, and the length (50 mm) was cut along the axis of alignment. The strips were then swollen in PBS before mechanical testing. Skeletal muscle was also cut into 10×50 mm strips, with the length (50 mm) parallel to the aligned native muscle fibers. The thickness was then trimmed to be homogenous throughout (5.2 ± 0.9 mm thickness). Samples were loaded into the mechanical testing apparatus, with a gauge length of 30 mm set. Samples were pulled at a rate of 10% strain/min to an extension of 12 mm in aqueous conditions. Before analysis, native muscle was conditioned to allow for proper alignment of collagen fibrils.[37] The tensile modulus was then calculated for all samples. Surface area was incorporated into calculations for stress to normalize for changes in thickness across samples.

Statistics

All data are expressed as mean ± standard deviation. The number of replicates used for each analysis is stated in the Results section below. To compare native muscle, dECM powder, and dECM scaffolds for biochemical analysis, a one-way analysis of variance (ANOVA) test was performed with posthoc analysis by Tukey's honestly significant difference (HSD). To investigate the effects of fiber alignment and crosslinking on fiber swelling, porosity, tensile modulus, and degradation kinetics, a two-way ANOVA test was performed with posthoc analysis by Tukey's HSD.

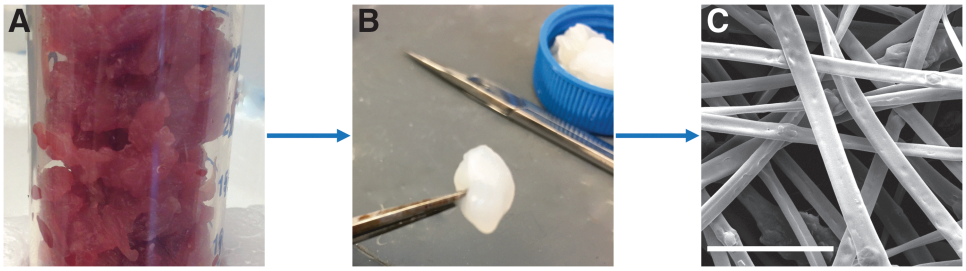

FIG. 1. Schematic of decellularization and production of dECM electrospun fibers. **(A)** Skeletal muscle was harvested from the hind limbs of New Zealand White rabbits and removed of all visible fascia and connective tissue. **(B)** Skeletal muscle was exposed to a number of reagents to remove cellular material from the extracellular matrix. **(C)** After homogenization and drying, dECM was electrospun without the use of a carrier polymer to form dECM fibers. The scale bar represents 10 μm. dECM, decellularized extracellular matrix.

Results

Decellularization of skeletal muscle tissue

Skeletal muscle from New Zealand White rabbits was harvested within 1 h of euthanasia, and all tissue was used right away. The skeletal muscle was cleared of fascia and connective tissue and cut into small pieces for processing (Fig. 1A). Skeletal muscle was decellularized using a number of reagents, including trypsin and washes in hypotonic and hypertonic salt solutions, to produce a white decellularized construct (Fig. 1B). Once decellularized, the muscle samples were much less stiff than muscle samples before processing. The dECM was then homogenized into a slurry, frozen, dried, and ground into a fine powder. The powder was then easily dispersed within HFIP that could be electrospun to produce microsized dECM fibers (Fig. 1C).

Biochemical characterization of dECM

To evaluate the quality of the dECM powder and dECM electrospun scaffolds, biochemical analysis was performed. Samples were lysed and solubilized to a workable form. To evaluate the DNA content within each sample, the DNA was first isolated and then measured via PicoGreen assay. As shown in Figure 2A, DNA is reduced ($p < 0.05$) after decellularization and milling to produce a course powder. DNA is further reduced ($p < 0.05$) after exposure to HFIP and electrospinning parameters. The DNA content fell

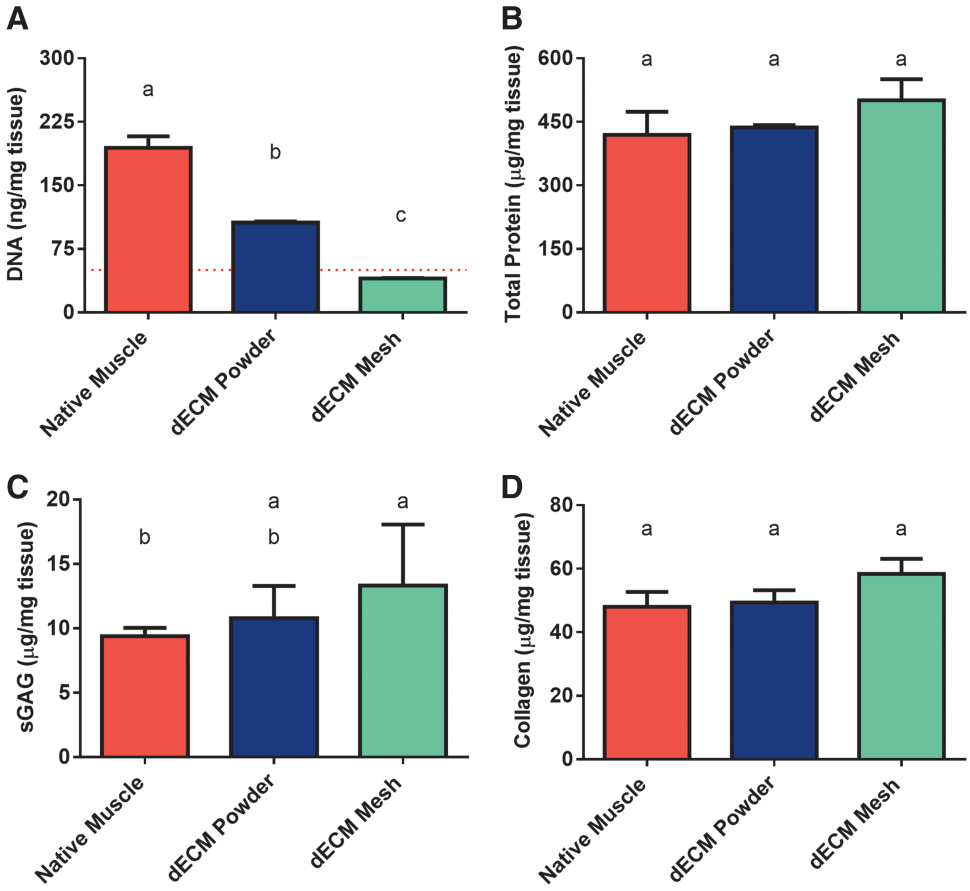

FIG. 2. Biochemical analysis of untreated (native) skeletal muscle, dECM powder, and dECM electrospun mesh. **(A)** DNA was quantified via PicoGreen assay. A *dashed red line* represents 50 ng/mg of tissue, which is the current recommended upper limit for decellularized material. **(B)** Total protein was quantified via BCA assay. **(C)** sGAG content was quantified via DMMB assay, and **(D)** collagen content was quantified via hydroxyproline assay. *Shared letters* indicate no significant difference between groups ($n = 3$, $p < 0.05$). BCA, bicinchoninic acid; sGAG, sulfated glycosaminoglycans; DMMB, 1,9-dimethylmethylene blue.

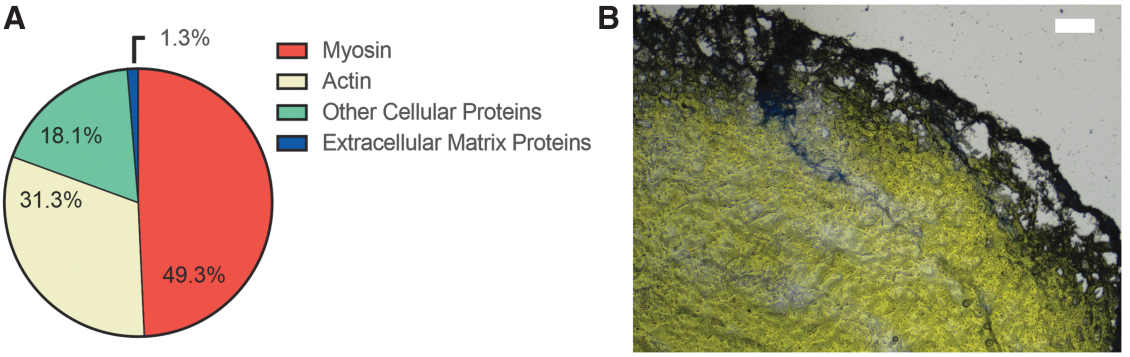

FIG. 3. Identification of proteins in decellularized muscle. Protein identification was performed on electrospun dECM scaffolds using LC-MS/MS **(A)**. Decellularized muscle was also evaluated histologically for collagen using an Alcian blue stain **(B)**.

below the recommended 50 ng of DNA/mg of dried tissue,[12,38] as denoted by a red line. The dECM mesh is in its final, usable form.

In addition to DNA, total protein, collagen, and sGAG were quantified for each sample group. Using a BCA assay, total protein was quantified. There was no significant difference ($p > 0.05$) between the total protein concentration of native muscle and that of dECM powder or electrospun dECM (Fig. 2B). Likewise, collagen concentration, measured indirectly through a hydroxyproline assay, did not differ ($p > 0.05$) between the untreated muscle sample and the two dECM groups (Fig. 2D). DMMB assay revealed no difference ($p > 0.05$) in sGAG concentration between dECM powder and electrospun dECM scaffolds (Fig. 2C), but the final electrospun form retained sGAG at a higher concentration than native muscle ($p < 0.05$).

When LC-MS/MS was run on electrospun dECM scaffolds, results reported that ECM proteins made up ~1.3% (Fig. 3A) of the total proteins within the tissue. Myosin and actin made up the majority of the proteins in the dECM scaffold. These results are further supported in the histological staining of collagen in the decellularized tissue construct shown in Figure 3B.

Evaluation of fiber swelling via confocal microscopy

Images were taken of dry and swollen dECM scaffolds via confocal microscopy. As shown in Figure 4C, AO fibers were slightly larger ($p < 0.05$) than RO fibers before swelling, but the mean fiber diameter for both groups was within 1 μm of each other. Representative images of swollen fibers are shown in Figure 4. RO and ROX fibers showed swelling in the range of 1–1.5 μm compared with the dry fibers. Crosslinked fibers (ROX and AOX) swelled significantly less ($p < 0.05$) than uncrosslinked fibers (RO and AO). Swollen RO and ROX fibers increased to ~2.8 μm (101% increase compared with dry RO) and 2.0 μm (43% increase compared with dry RO), respectively. Swollen AO and AOX fibers increased to ~3.5 μm (70% increase compared with dry AO) and 2.7 μm (33% increase compared with dry AO), respectively. Swollen fibers in all four dECM groups had significantly larger ($p < 0.05$) fiber diameters than their dry controls.

Evaluation of bulk scaffold swelling

The change in thickness and diameter of dECM scaffolds after swelling in PBS was evaluated. As shown in Figure 5, the mean thickness and diameter of swollen, uncrosslinked dECM scaffolds were lower than the dry counterparts. ROX swollen normalized thickness (~96%) was significantly higher ($p < 0.05$) than RO swollen thickness (~49%). There was no significant difference ($p > 0.05$) in the swollen normalized thickness of AO (~85%) and AOX (~63%) scaffolds. The dry scaffold thickness of RO, ROX, AO, and AOX scaffolds was ~46, 50, 95, and 72 μm, respectively.

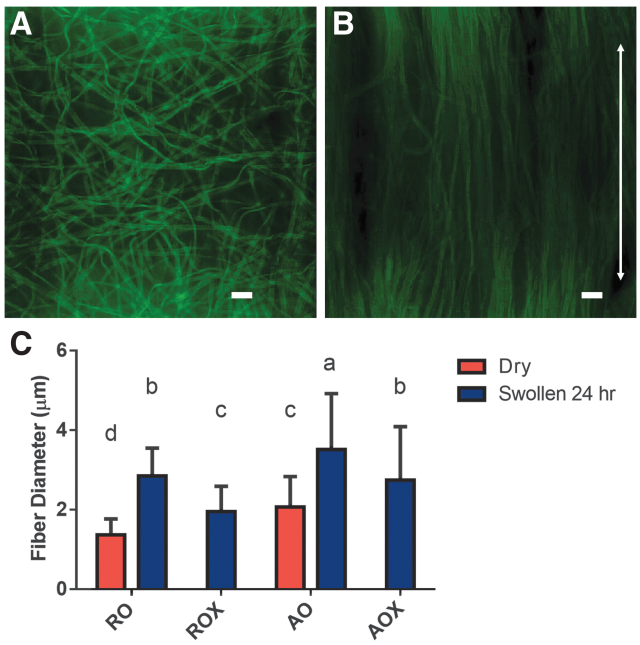

FIG. 4. Analysis of fiber swelling. **(A)** Representative images of swollen random (RO) dECM fibers and **(B)** swollen aligned (AO) dECM fibers were taken. The scale bar represents 10 μm. The *arrow* represents the direction of fiber orientation. **(C)** Fiber diameter was measured dry (*red bars*) and after 24 h of swelling in PBS (*blue bars*). *Shared letters* indicate no significant difference between groups ($n \geq 50$, $p < 0.05$). PBS, phosphate-buffered saline.

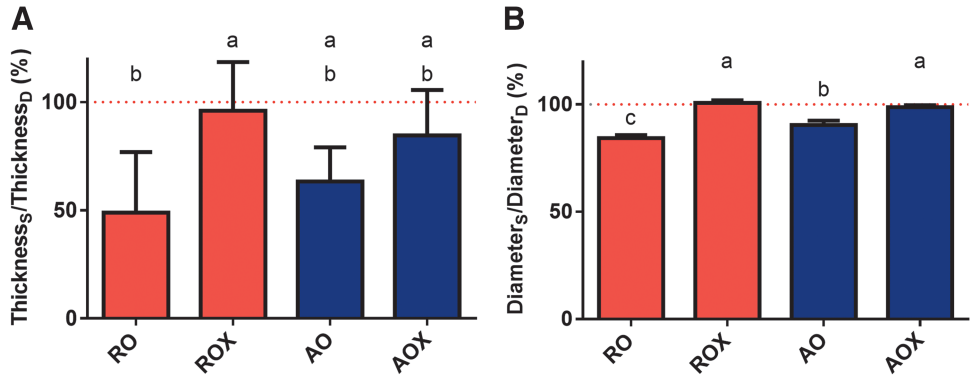

FIG. 5. Bulk swelling of dECM scaffolds. **(A)** Scaffold thickness and **(B)** diameter were measured dry and after swelling for 24 h in PBS. Thickness and diameter are represented as swollen/dry as a percentage. The *dashed red line* represents 100% or no change in the swollen parameter compared to dry. *Shared letters* indicate no significant difference between groups ($n=5$, $p<0.05$). (Thickness$_s$ = swollen scaffold thickness, Thickness$_D$ = dry scaffold thickness, Diameter$_s$ = swollen scaffold diameter, Diameter$_D$ = dry scaffold diameter.)

The scaffold diameter of swollen dECM scaffolds followed a similar trend. The normalized diameter of swollen ROX scaffolds (~101%) was significantly higher ($p<0.05$) than RO scaffolds (~84%). Similarly, the normalized diameter of swollen AOX scaffolds (~99%) was significantly higher ($p<0.05$) than AO scaffolds (~90%).

Porosity of dECM scaffolds

Porosity is very important for tissue engineering scaffolds to allow for nutrient and metabolic waste exchange. The porosity of dECM scaffolds was measured dry and after swelling in PBS. As expected, the porosity of dECM scaffolds was very high for RO (87.6%) and AO (86.5%) scaffolds when dry (Fig. 6). Production of high-porosity scaffolds is one of the characteristics of electrospinning. The porosity of dry RO scaffolds was slightly higher ($p<0.05$) than dry AO scaffolds. When the scaffolds were swollen, there was an overall decrease in the porosity regardless of crosslinking or fiber orientation. There was a significant reduction in porosity ($p<0.05$) after swelling in RO and ROX scaffolds compared with the dry control. The porosity of swollen, RO scaffolds

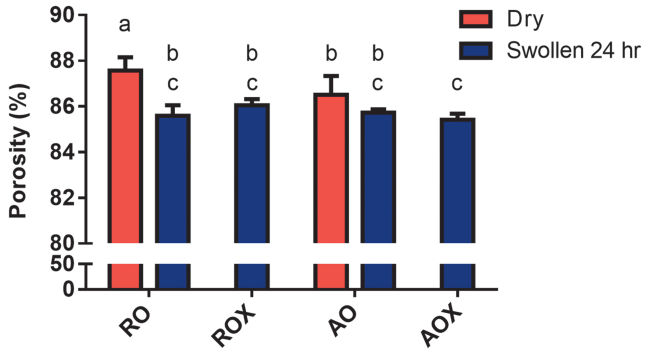

FIG. 6. Porosity of dECM scaffolds. The porosity of randomly oriented (RO, ROX) and aligned (AO, AOX) dECM scaffolds was analyzed dry and after swelling in PBS via confocal microscopy and image processing software (ImageJ). The porosity of dry (*red bars*) and swollen (*blue bars*) is presented as a percentage. *Shared letters* indicate no significant difference between groups ($n\geq25$, $p<0.05$).

decreased ($p<0.05$) to 85.6% (2.3% decrease compared with dry RO) and ROX scaffolds decreased ($p<0.05$) to 86.0% (1.7% decrease compared with dry RO). The porosity of swollen, AO scaffolds changed to 85.7%, but there was no significant difference observed ($p>0.05$). The porosity of AOX scaffolds decreased ($p<0.05$) to 85.4% (1.3% decrease compared with dry AO).

Degradation kinetics of dECM scaffolds

Scaffolds from all four groups were exposed to degradation media and incubated at 37°C under mild agitation to study the passive degradation kinetics (hydrolysis) and active degradation kinetics (enzymatic degradation) of dECM scaffolds. In only 6 h of exposure to PBS, there was ~15% mass loss in the RO scaffolds, 12% mass loss in the ROX scaffolds, 28% mass loss in the AO scaffolds, and 23% mass loss in the AOX scaffolds (Fig. 7A). Comparisons were drawn to study the effects of crosslinking and fiber orientation on the degradation kinetics. The results of statistical analysis can be found in Supplementary Figure S2. There was no significant decrease ($p>0.05$) observed in the mass of ROX scaffolds throughout the 8-week study in PBS. However, there was a significant decrease ($p<0.05$) in RO scaffold mass throughout the study. At the completion of the study, ~3% of the scaffold mass remained. This was the greatest reduction in mass of all the groups in the PBS study. Similarly, there was a much greater reduction in mass in the AO scaffolds compared with the AOX scaffolds. At the end of the 8-week PBS study, only 13% of the original mass remained in the AO group, while 44% of the original mass remained in the AOX group. Overall, the greatest rate of mass loss for all groups was observed in the first 6 h of the study. A mass loss rate of ~2.7% mass/h was observed in the RO scaffolds in the first 6 h in PBS, 2% in the ROX scaffolds, 4.7% in the AO scaffolds, and 3.9% in the AOX scaffolds.

Scaffolds were placed in PBS supplemented with collagenase (125 U/mL) and incubated under the same conditions as in the PBS-alone groups to model enzyme-mediated degradation. In 6 h, there was ~58% mass loss observed in the RO scaffolds, 9% mass loss in the ROX scaffolds, 51% in the AO scaffolds, and 46% in the AOX scaffolds (Fig. 7B). In

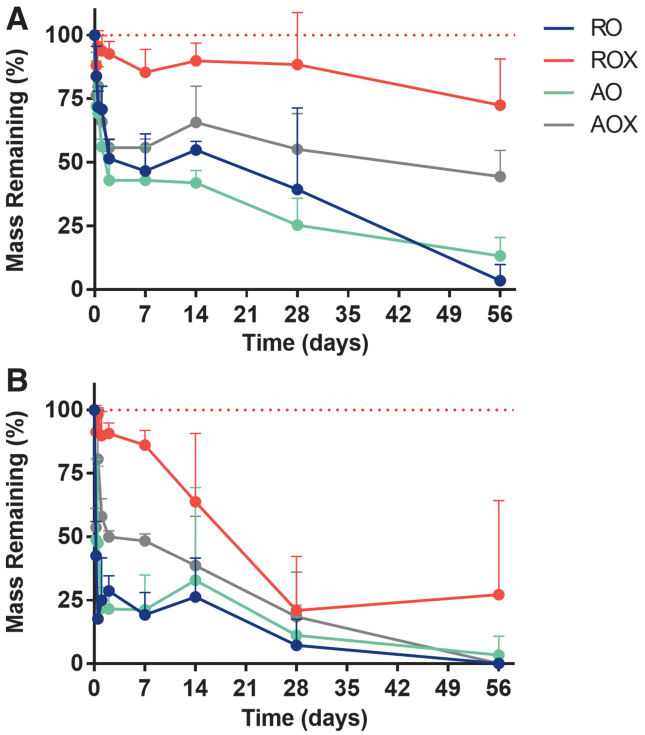

FIG. 7. Degradation kinetics of dECM scaffolds. **(A)** PBS degradation of dECM scaffolds and **(B)** PBS supplemented with collagenase degradation of dECM scaffolds. A *dashed red line* represents 100% mass remaining. Four groups of dECM scaffolds ($n=5$) (RO, ROX, AO, and AOX) were tested under mild agitation and incubation at 37°C. Statistics is shown in Supplementary Figure S2.

addition, only the ROX scaffolds showed a substantial amount of mass remaining after 8 weeks in collagenase solution. All of scaffolds were either completely degraded or nearly completely degraded by the end of the study. Similar to the PBS-only study, the mass loss rates of scaffolds exposed to collagenase were greatest in the first 6 h of the study. A mass loss rate of ~9.6% mass/h was observed in the RO scaffolds in the first 6 h in collagenase solution, 1.5% mass/h in the ROX scaffolds, 8.5% mass/h in the AO scaffolds, and 7.7% mass/h in the AOX scaffolds.

Mechanical testing of dECM scaffolds

Uniaxial tensile testing was performed on native skeletal muscle that was harvested from New Zealand White rabbits as well as dECM scaffolds from each of the four groups. dECM scaffolds were tested with a gauge length of 30 mm and were pulled at a rate of 10% strain/min. The native skeletal muscle had a mean tensile modulus of ~116 kPa. As shown in Figure 8, ROX dECM scaffolds (185 kPa) had a significantly higher ($p<0.05$) tensile modulus than RO scaffolds (44 kPa). However, neither random dECM scaffold group was significantly different ($p>0.05$) from native skeletal muscle. Aligned dECM scaffolds had a significantly higher ($p<0.05$) tensile modulus than native skeletal muscle. The tensile modulus of AO scaffolds was not significantly different ($p>0.05$) from ROX scaffolds. However, AOX scaffolds (850 kPa) had a significantly higher ($p<0.05$) tensile modulus than AO scaffolds (213 kPa).

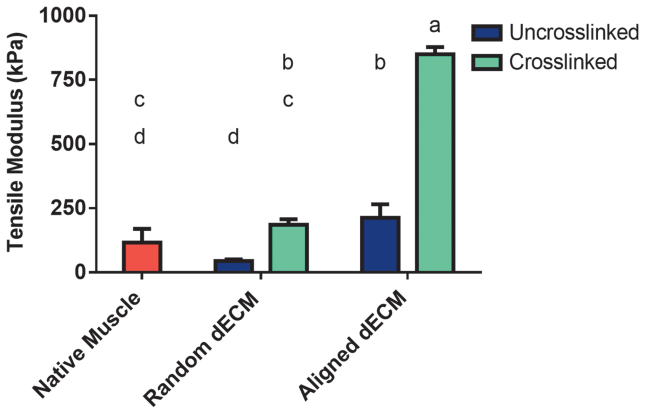

FIG. 8. Tensile modulus of dECM scaffolds. Scaffolds were tested on a uniaxial mechanical tester and pulled at 10% strain/min. The tensile modulus was then calculated for four groups of dECM scaffolds and native skeletal. Uncrosslinked scaffolds are represented by a *blue bar* and crosslinked scaffolds by a *green bar*. Native skeletal muscle is represented by a *red bar*. *Shared letters* indicate no significant difference between groups ($n=5$, $p<0.05$).

Discussion

Over the course of this study, we have developed a novel procedure for the fabrication of electrospun dECM scaffolds without the need for a carrier polymer. In addition, we have characterized the biochemical composition and the material properties of the dECM scaffolds. Scaffolds derived completely from ECM are advantageous over other natural and hybrid scaffolds because they better mimic the native cell microenvironment.[33] In addition, natural polymers electrospun in HFIP have been shown to retain bioactivity.[39–41] Skeletal muscle harvested from the hind limbs of New Zealand White rabbits was exposed to a number of different decellularization reagents that have been shown to be effective enough to remove cellular material from skeletal muscle but gentle enough to retain ECM components that are important for future applications in cell recruitment, cell adhesion, cell signaling and differentiation, and scaffold integration. Several established decellularization protocols were attempted,[10,11,13] but we found that using trypsin, Triton X-100, and a series of hypotonic and hypertonic solutions was effective in removing DNA (Fig. 2A) while retaining ECM components. In addition, many traditional decellularization protocols for skeletal muscle incorporate several washes in sodium dodecyl sulfate (SDS), which can be cytotoxic if not removed fully from the matrix.[42]

As shown in Figure 2, there was no significant difference ($p>0.05$) in the total protein and collagen concentrations in dECM electrospun scaffolds compared with native skeletal muscle. This is important for cell adhesion, growth, and differentiation onto dECM scaffolds for future *in vitro* and *in vivo* studies.[1,17,43,44] While the hydroxyproline assay is an indirect measure of collagen content, we believe that LC-MS/MS is a better method for identifying the proteins and relative amount of proteins present within the electrospun dECM scaffolds. This powerful technique allows for a more thorough understanding of the composition of these scaffolds. We had a low concentration of collagen (1.0% ± 0.5%) and other ECM proteins (1.3% ± 0.7%) present within the

decellularized scaffolds (Fig. 3 and Supplementary Table S1). We believe that this is because of the mild decellularization methods used in this study, which allowed for high retention of cellular proteins myosin and actin. This study provides an in-depth analysis of the protein composition of dECM scaffolds, which is not captured in many other studies using decellularized tissues. While we did not anticipate that myosin would be present in such large quantities in dECM scaffolds, similar trends may have been overlooked in other studies that did not fully examine the protein makeup of their decellularized tissues. The ECM proteins present in electrospun dECM scaffolds were predominantly collagen (I, III, IV, V, VI, VII, and XV), laminin, keratin, and fibronectin. A full list of the proteins identified through LC-MS/MS can be found in Supplementary Table S1.

In addition, the concentration of sGAG remained approximately the same throughout the decellularization process. We hypothesize that the slight increase in sGAG concentration in the electrospun dECM compared with native muscle can be attributed to the loss of a matrix component not analyzed in this study. sGAG concentrations are especially important for cell signaling and differentiation because growth factors are thought to be sequestered in sGAG.[45,46] Growth factors within skeletal muscle dECM have been shown to drive myogenic differentiation, neurogenic differentiation, and angiogenic differentiation.[2,17] Each of these pathways is important for regeneration of skeletal muscle *in vivo*.

Decellularized skeletal muscle has been used in a number of different forms in the last several years. Most commonly, hydrated dECM pieces have been cut to fit a defect and sutured into place.[2,16,17] While the dECM has been shown to drive differentiation, there are several limitations—size, shape, and physicochemical properties of the dECM are difficult to control and modulate to fit specific defects and applications. For this reason, we have chosen to combine dECM with electrospinning to create a high-throughput approach to fabricating dECM scaffolds with tunable physicochemical properties while retaining the biochemical cues of native skeletal muscle.

Previous studies with electrospinning dECM have relied on blending with carrier polymers.[27–32] We have identified key steps that are crucial for the successful formation of stable, electrospun dECM scaffolds. By homogenizing the dECM into a uniform slurry, any remaining connective tissue could be effectively removed. Sieving dried dECM was also used so that only small particles (<300 μm) were included in electrospinning solutions. When analyzed, it was found that $96.1\% \pm 1.1\%$ of ground dECM passed through a 300 μm sieve, and sieved particles were irregularly shaped with a diameter of 166.6 ± 81.4 μm ($n = 5$ fields and $n \geq 10$ particles per field). It was found that without sieving, a thick electrospinning solution resulted, which did not create fibers. Rather, a gel-like material deposited and grew on the end of the electrospinning needle. Likewise, if the dECM was not homogenized, the same phenomenon was observed, regardless of if sieving was performed. We hypothesized that connective tissues impede the formation of homogenous dECM electrospinning solution and the subsequent formation of dECM fibers. In addition, we hypothesize that small particles are required to limit the interactions of dECM proteins and keep dECM in suspension in HFIP rather than clumping together or dissolving to form a gel-like material. Furthermore, we believe that the decellularization process and the ECM components that are retained impact the behavior of the electrospinning solution. When SDS was used, the dECM was more likely to dissolve in HFIP and form a gel-like material.

The fabrication of dECM scaffolds through electrospinning allows for modulation of physicochemical properties during fabrication (fiber orientation) and after fabrication through crosslinking. As shown in Figure 4C, dECM fibers used in this study were on the microscale. While 10% dECM/HFIP was used for the duration of this study, lower concentrations were experimented with to create smaller electrospun fibers (data not shown). We hypothesize that fiber diameters can further be modulated by adjusting the polymer concentration, flow rate, and voltages used to create larger or smaller fibers.[21,47] In addition, the fiber orientation of dECM fibers was modulated by changing the electrospinning setup. RO fibers were fabricated by collecting onto a stationary copper collector. Fibers were aligned when electrospun on a rotating collector. For muscle, aligned fibers provide an important framework to guide myogenic differentiation and promote the formation of mature myotubes.[48,49] Electrospun dECM fibers are unique in that they are stable without the need of crosslinking. Gelatin and collagen typically require a crosslinking step or blending with a synthetic polymer to allow for stability and long-term use.[24,26,50] We hypothesize that the electrospun dECM retains some of the solubility properties of native muscle, allowing for decreased solubility in saline solution. As shown from the degradation study performed (Fig. 7A), uncrossinked dECM scaffolds can last up to 8 weeks in PBS.

Fiber swelling occurred in all dECM groups. However, swollen RO and AO scaffolds showed larger fiber diameters than swollen ROX and AOX scaffolds, respectively (Fig. 4C). In addition, mean scaffold thickness and diameter were higher in crosslinked scaffolds than their uncrosslinked counterparts (Fig. 5). However, the porosity of swollen scaffolds did not vary with fiber alignment or crosslinking (Fig. 6). These findings suggest that crosslinking helps to retain fiber structure. We hypothesize that the lower mechanical properties of uncrosslinked scaffolds (Fig. 8) contributed to the decrease in scaffold thickness and diameter on swelling. The degradation study performed also suggests that loss of mass occurs within the first 24 h of uncrosslinked scaffolds being exposed to PBS, which may attribute to the reduction in scaffold thickness and diameter. In addition, AO and AOX fibers were found to swell less than RO and ROX fibers, respectively. These findings suggest that fiber topography influences the degree of fiber swelling.

Degradation kinetics is very important when using a material as an implant *in vivo*. As shown in Figure 7, mass loss throughout groups was highest in the first 6 h of exposure to degradation media. We hypothesize that dissolution of the matrix proteins was occurring in the PBS groups and enzyme-mediated dissolution was occurring in the collagenase groups. In addition, we hypothesize that degradation occurred in later time points due to the steady loss of mass observed, but no analysis of media by-products was performed. All dECM groups were retained up to 8 weeks in PBS. This is unique for natural materials, as gelatin and collagen typically require crosslinking for long-term culture. In addition, uncrosslinked scaffolds were retained in collagenase for 4 weeks. This

indicates that uncrosslinked dECM scaffolds could be considered potential candidates for long-term *in vitro* culture and use in *in vivo* studies for muscle repair.

However, confocal analysis of fiber morphology in degradation media showed that the fiber structure of the uncrosslinked dECM scaffolds was greatly decreased after 7 days in collagenase solution (Supplementary Fig. S3). The ROX scaffolds were substantially retained in PBS and in collagenase. In addition to the effects of the crosslinking agent, glutaraldehyde, stabilizing the electrospun matrix, we hypothesize that the stability of the electrospun dECM scaffolds is due to the gelation of collagen fibrils during electrospinning and the stabilizing interactions of ECM components. During electrospinning, fibers fuse at the intersection of two fibers as the solvent dries, and collagen organizes itself into fibrils through fibrillogenesis.[51] We hypothesize that this physical interaction and interactions of ECM proteins, including fibrillar collagen, small leucine-rich proteoglycans, membrane-associated collagens with interrupted triple-helices, fibril-associated collagen with interrupted triple-helices, and basement membrane proteins, hold the matrix together. While the tensile modulus of ROX scaffolds was lower than that of AOX scaffolds, we hypothesize that the stability was increased due to the high number of fibers that intersected within ROX scaffolds, allowing for more stable crosslinks and an isotropic behavior.[52] Overall, a higher rate of mass loss was observed in RO and AO scaffolds than ROX and AOX scaffolds, respectively, suggesting that crosslinking retains the scaffold structure and slows dECM dissolution and long-term degradation.[24]

As shown in Figure 8, AO fibers had a significantly higher tensile modulus than RO fibers. This parameter can be further tuned by varying the degree of alignment, which can be controlled by adjusting the rate at which the mandrel turns. The tensile modulus of dECM scaffolds was further increased by crosslinking scaffolds. The groups reported here were at both extremes (no crosslinking and high levels of crosslinking). However, we hypothesize that the amount of time that scaffolds are exposed to glutaraldehyde vapor will be directly related to the tensile modulus of that scaffold. The RO scaffolds were in the tensile modulus range of native muscle, while the AO scaffolds had higher ($p < 0.05$) tensile moduli than native muscle (Fig. 8). However, we hypothesize that lowering the degree of alignment will decrease the tensile modulus.[53]

While there have been studies performed that use dECM blended with carrier polymers to create electrospun scaffolds,[28] to our knowledge, this is the first account of the formation and characterization of stable electrospun scaffolds fabricated without the need for a carrier polymer. These materials are highly tunable and show great promise as scaffolds for applications such as VML. While the extremes were used in this study, we hypothesize that decreasing the fiber alignment would result in tensile mechanical properties between RO scaffolds and AO scaffolds. Similarly, decreasing the crosslinking would result in degradation kinetics between RO scaffolds and ROX scaffolds.[54] In addition, we believe that this technology will establish a foundation for the formation of biomaterials derived from dECM and used in diverse tissue engineering applications.

Conclusions

In this study, we developed a novel, high-throughput method to fabricate muscle dECM scaffolds through electrospinning. We have demonstrated successful decellularization of skeletal muscle tissue and retention of key ECM components for our dECM scaffolds. In addition, we identified steps that are pivotal for the successful formation of stable, electrospun muscle dECM scaffolds without the need for a carrier polymer. Our decellularization protocol relies on Triton X-100 and hypotonic/hypertonic salt solutions to remove DNA rather than SDS. The homogenization of decellularized skeletal muscle and the removal of dECM particles larger than 300 μm were found to be pivotal for the successful production of dECM fibers. These steps allowed for appropriate interactions between skeletal muscle proteins to form electrospun fibers without the need for a carrier polymer. In addition, the resulting dECM scaffolds were less soluble than other natural electrospun materials due to the limited solubility of muscle proteins. Without crosslinking, dECM scaffolds were retained in PBS for 8 weeks. The electrospun dECM scaffolds had high porosity, which is necessary to facilitate transport of nutrients and metabolic waste. Uncrosslinked dECM scaffolds had tensile moduli in the range of native skeletal muscle (~ 100 kPa), and mechanical properties were increased through fiber alignment and crosslinking. Electrospinning has allowed us to control fiber orientation, mechanical properties, and degradation kinetics, which affect cell attachment, migration, and differentiation. Electrospinning dECM leverages the biochemical cues of native muscle with the capacity to tune physicochemical properties.

Acknowledgments

We acknowledge support toward the development of dECM scaffolds from the National Institutes of Health (P41 EB023833). We also acknowledge support from a National Science Foundation Graduate Research Fellowship (MMS), a Ford Foundation Predoctoral Research Fellowship (MMS), and a Ruth L. Kirschstein Fellowship from the National Institute of Dental and Craniofacial Research (EW, F31 DE027586). We also thank Joohyun Lim in the laboratory of Dr. Brendan Lee at Baylor College of Medicine, Dr. Stephen Mills at the University of Texas Health Science Center, and Shail Mehta in the laboratory of Dr. Jane Grande-Allen for their assistance.

Disclosure Statement

No competing financial interests exist.

Supplementary Material

Supplementary Figure S1
Supplementary Figure S2
Supplementary Figure S3
Supplementary Table S1

References

1. Turner, N.J., and Badylak, S.F. Regeneration of skeletal muscle. Cell Tissue Res **347,** 759, 2012.

2. Dziki, J., Badylak, S., Yabroudi, M., et al. An acellular biologic scaffold treatment for volumetric muscle loss: results of a 13-patient cohort study. NPJ Regen Med **1,** 16008, 2016.
3. Grogan, B.F., and Hsu, J.R. Volumetric muscle loss. J Am Acad Orthop Surg **19 Suppl 1,** S35, 2011.
4. Wu, X., Corona, B.T., Chen, X., and Walters, T.J. A standardized rat model of volumetric muscle loss injury for the development of tissue engineering therapies. Biores Open Access **1,** 280, 2012.
5. Tzu, M., Li, A., Willett, N.J., Uhrig, B.A., Guldberg, R.E., and Warren, G.L. Functional analysis of limb recovery following autograft treatment of volumetric muscle loss in the quadriceps femoris. J Biomech **47,** 2013, 2014.
6. Shah, K., Majeed, Z., Jonason, J., and O'Keefe, R.J. The role of muscle in bone repair: the cells, signals, and tissue responses to injury. Curr Osteoporos Rep **11,** 130, 2013.
7. Davis, K.M., Griffin, K.S., Chu, T.G., et al. Muscle-bone interactions during fracture healing. J Musculoskelet Neuronal Interact **15,** 1, 2015.
8. Liao, J., Guo, X., Grande-Allen, K.J., Kasper, F.K., and Mikos, A.G. Bioactive polymer/extracellular matrix scaffolds fabricated with a flow perfusion bioreactor for cartilage tissue engineering. Biomaterials **31,** 8911, 2010.
9. Smoak, M.M., Pearce, H.A., and Mikos, A.G. Microfluidic devices for disease modeling in muscle tissue. Biomaterials **198,** 250, 2019.
10. Fu, Y., Fan, X., Tian, C., et al. Decellularization of porcine skeletal muscle extracellular matrix for the formulation of a matrix hydrogel: a preliminary study. J Cell Mol Med **20,** 740, 2016.
11. Rao, N., Agmon, G., Tierney, M.T., et al. Engineering an injectable muscle-specific microenvironment for improved cell delivery using a nanofibrous extracellular matrix hydrogel. ACS Nano **11,** 3851, 2017.
12. Ungerleider, J.L., Johnson, T.D., Rao, N., and Christman, K.L. Fabrication and characterization of injectable hydrogels derived from decellularized skeletal and cardiac muscle. Methods **84,** 53, 2015.
13. Wassenaar, J.W., Braden, R.L., Osborn, K.G., and Christman, K.L. Modulating in vivo degradation rate of injectable extracellular matrix hydrogels. J Mater Chem B **4,** 2794, 2016.
14. Choi, Y.-J., Kim, T.G., Jeong, J., Yi, H.-G., Park, J.W., Hwang, W., and Cho, D.-W. 3D cell printing of functional skeletal muscle constructs using skeletal muscle-derived bioink. Adv Healthc Mater **5,** 2636, 2016.
15. Hinderer, S., Layland, S.L., and Schenke-Layland, K. ECM and ECM-like materials - Biomaterials for applications in regenerative medicine and cancer therapy. Adv Drug Deliv Rev **97,** 260, 2016.
16. Wolf, M.T., Daly, K.A., Reing, J.E., and Badylak, S.F. Biologic scaffold composed of skeletal muscle extracellular matrix. Biomaterials **33,** 2916, 2012.
17. Sicari, B.M., Rubin, J.P., Dearth, C.L., et al. An acellular biologic scaffold promotes skeletal muscle formation in mice and humans with volumetric muscle loss. Sci Transl Med **6,** 234ra58, 2014.
18. Agmon, G., and Christman, K.L. Controlling stem cell behavior with decellularized extracellular matrix scaffolds. Curr Opin Solid State Mater Sci **20,** 193, 2016.
19. Rothrauff, B.B., Yang, G., and Tuan, R.S. Tissue-specific bioactivity of soluble tendon-derived and cartilage-derived extracellular matrices on adult mesenchymal stem cells. Stem Cell Res Ther **8,** 133, 2017.
20. Saraf, A., Baggett, L.S., Raphael, R.M., Kasper, F.K., and Mikos, A.G. Regulated non-viral gene delivery from coaxial electrospun fiber mesh scaffolds. J Control Release **143,** 95, 2010.
21. Pham, Q.P., Sharma, U., and Mikos, A.G. Electrospun poly(ε-caprolactone) microfiber and multilayer nanofiber/microfiber scaffolds: characterization of scaffolds and measurement of cellular infiltration. Biomacromolecules **7,** 2796, 2006.
22. Deitzel, J., Kleinmeyer, J., Harris, D., and Beck Tan, N. The effect of processing variables on the morphology of electrospun nanofibers and textiles. Polymer (Guildf) **42,** 261, 2001.
23. Gong, W., Lei, D., Li, S., et al. Hybrid small-diameter vascular grafts: anti-expansion effect of electrospun poly ε-caprolactone on heparin-coated decellularized matrices. Biomaterials **76,** 359, 2016.
24. Kishan, A.P., Nezarati, R.M., Radzicki, C.M., et al. In situ crosslinking of electrospun gelatin for improved fiber morphology retention and tunable degradation. J Mater Chem B **3,** 7930, 2015.
25. Laha, A., Sharma, C.S., and Majumdar, S. Sustained drug release from multi-layered sequentially crosslinked electrospun gelatin nanofiber mesh. Mater Sci Eng C **76,** 782, 2017.
26. Ko, J.H., Yin, H., An, J., et al. Characterization of crosslinked gelatin nanofibers through electrospinning. Macromol Res **18,** 137, 2010.
27. Francis, M.P., Sachs, P.C., Madurantakam, P.A., et al. Electrospinning adipose tissue-derived extracellular matrix for adipose stem cell culture. J Biomed Mater Res A **100,** 1716, 2012.
28. Baiguera, S., Del Gaudio, C., Lucatelli, E., et al. Electrospun gelatin scaffolds incorporating rat decellularized brain extracellular matrix for neural tissue engineering. Biomaterials **35,** 1205, 2014.
29. Levorson, E.J., Raman Sreerekha, P., Chennazhi, K.P., Kasper, F.K., Nair, S.V., and Mikos, A.G. Fabrication and characterization of multiscale electrospun scaffolds for cartilage regeneration. Biomed Mater **8,** 14103, 2013.
30. Zhong, S., Teo, W.E., Zhu, X., Beuerman, R.W., Ramakrishna, S., and Yung, L.Y.L. An aligned nanofibrous collagen scaffold by electrospinning and its effects on in vitro fibroblast culture. J Biomed Mater Res A **79,** 456, 2006.
31. Young, B.M., Shankar, K., Allen, B.P., et al. Electrospun decellularized lung matrix scaffold for airway smooth muscle culture. ACS Biomater Sci Eng **3,** 3480, 2017.
32. Schoen, B., Avrahami, R., Baruch, L., et al. Electrospun extracellular matrix: paving the way to tailor-made natural scaffolds for cardiac tissue regeneration. Adv Funct Mater **27,** 1700427, 2017.
33. Coenen, A.M.J., Bernaerts, K.V, Harings, J.A.W., Jockenhoevel, S., and Ghazanfari, S. Elastic materials for tissue engineering applications: natural, synthetic, and hybrid polymers. Acta Biomater **79,** 60, 2018.
34. Dahlin, R.L., Ni, M., Meretoja, V.V, Kasper, F.K., and Mikos, A.G. TGF-β3-induced chondrogenesis in co-cultures of chondrocytes and mesenchymal stem cells on biodegradable scaffolds. Biomaterials **35,** 123, 2014.
35. Stegemann, H., and Stalder, K. Determination of hydroxyproline. Clin Chim Acta **18,** 267, 1967.
36. Singelyn, J.M., and Christman, K.L. Modulation of material properties of a decellularized myocardial matrix scaffold. Macromol Biosci **11,** 731–738, 2011.

37. Kammoun, M., Pouletaut, P., Canon, F., et al. Impact of TIEG1 deletion on the passive mechanical properties of fast and slow twitch skeletal muscles in female mice. PLoS One **11,** e0164566, 2016.
38. Reing, J.E., Brown, B.N., Daly, K.A., et al. The effects of processing methods upon mechanical and biologic properties of porcine dermal extracellular matrix scaffolds. Biomaterials **31,** 8626, 2010.
39. Kwon, I.K., and Matsuda, T. Co-Electrospun nanofiber fabrics of Poly(l-lactide-co-ε-caprolactone) with type I collagen or heparin. Biomacromolecules **6,** 2096, 2005.
40. Stitzel, J., Liu, J., Lee, S.J., et al. Controlled fabrication of a biological vascular substitute. Biomaterials **27,** 1088, 2006.
41. Stankus, J.J., Guan, J., and Wagner, W.R. Fabrication of biodegradable elastomeric scaffolds with sub-micron morphologies. J Biomed Mater Res A **70,** 603, 2004.
42. Crapo, P.M., Gilbert, T.W., and Badylak, S.F. An overview of tissue and whole organ decellularization processes. Biomaterials **32,** 3233, 2011.
43. Badylak, S.F., Dziki, J.L., Sicari, B.M., Ambrosio, F., Boninger, M.L. Mechanisms by which acellular biologic scaffolds promote functional skeletal muscle restoration. Biomaterials **103,** 128, 2016.
44. Braun, T., and Gautel, M. Transcriptional mechanisms regulating skeletal muscle differentiation, growth and homeostasis. Nat Rev Mol Cell Biol **12,** 349, 2011.
45. Vlodavsky, I., Folkman, J., Sullivan, R., Fridman, R., Ishai-Michaeli, R., Sasse, J. and Klagsbrun, M. Endothelial cell-derived basic fibroblast growth factor: synthesis and deposition into subendothelial extracellular matrix. Proc Natl Acad Sci USA **84,** 2292, 1987.
46. Vlodavsky, I., Miao, H.-Q., Medalion, B., Danagher, P., and Ron, D. Involvement of heparan sulfate and related molecules in sequestration and growth promoting activity of fibroblast growth factor. Cancer Metastasis Rev **15,** 177, 1996.
47. Pham, Q.P., Sharma, U., and Mikos, A.G. Electrospinning of polymeric nanofibers for tissue engineering applications: a review. Tissue Eng **12,** 1197, 2006.
48. Qazi, T.H., Mooney, D.J., Pumberger, M., Geißler, S., and Duda, G.N. Biomaterials based strategies for skeletal muscle tissue engineering: existing technologies and future trends. Biomaterials **53,** 502, 2015.
49. Mertens, J.P., Sugg, K.B., Lee, J.D., and Larkin, L.M. Engineering muscle constructs for the creation of functional engineered musculoskeletal tissue. Regen Med **9,** 89, 2014.
50. Patel, Z.S., Ueda, H., Yamamoto, M., Tabata, Y., and Mikos, A.G. In vitro and in vivo release of vascular endothelial growth factor from gelatin microparticles and biodegradable composite scaffolds. Pharm Res **25,** 2370, 2008.
51. Buttafoco, L., Kolkman, N.G., Engbers-Buijtenhuijs, P., et al. Electrospinning of collagen and elastin for tissue engineering applications. Biomaterials **27,** 724, 2006.
52. Orr, S.B., Chainani, A., Hippensteel, K.J., et al. Aligned multilayered electrospun scaffolds for rotator cuff tendon tissue engineering. Acta Biomater **24,** 117, 2015.
53. Chen, F., Su, Y., Mo, X., He, C., Wang, H., and Ikada, Y. Biocompatibility, alignment degree and mechanical properties of an electrospun chitosan-P(LLA-CL) fibrous scaffold. J Biomater Sci Polym Ed **20,** 2117, 2009.
54. Zhu, B., Li, W., Chi, N., Lewis, R.V., Osamor, J., and Wang, R. Optimization of glutaraldehyde vapor treatment for electrospun collagen/silk tissue engineering scaffolds. ACS Omega **2,** 2439, 2017.

Address correspondence to:
Antonios G. Mikos, PhD
Department of Bioengineering
Rice University
6500 Main Street, MS-142
Houston, TX 77030

E-mail: mikos@rice.edu

Received: November 29, 2018
Accepted: March 6, 2019
Online Publication Date: May 13, 2019